AMBER/VLTI observations of Eta Carinae with high spatial resolution and spectral resolutions of $\lambda/\triangle\lambda = 1\,500$ and $12\,000$ [*]

G. Weigelt [a], T. Driebe [a], K.-H. Hofmann [a], S. Kraus [a],
R. Petrov [b], D. Schertl [a],

[a] *Max-Planck-Institut für Radioastronomie, Auf dem Hügel 69, D-53121 Bonn, Germany*

[b] *Laboratoire Universitaire d'Astrophysique de Nice, UMR 6525 Université de Nice/CNRS, Parc Valrose, F-06108 Nice cedex 2, France*

Abstract

We present the first NIR interferometric observations of the LBV η Carinae with high spectral resolution (Weigelt et al., 2006, astro-ph/0609715). Our observations demonstrate the potential of AMBER/VLTI to unveil new structures on the scales of milliarcseconds. The aim of this work is to study the wavelength dependence of η Car's optically thick wind region with a high spatial resolution of 5 mas (11 AU) and high spectral resolution. The observations were carried out with three 8.2 m VLTI Unit Telescopes. The raw data are interferograms obtained with spectral resolutions of $\lambda/\triangle\lambda = 1\,500$ (MR-K mode) and $12\,000$ (HR-K mode). The observations were performed in the wavelength range around both the He I $2.059\,\mu$m and the Brγ $2.166\,\mu$m emission lines. The spectrally dispersed AMBER interferograms allow us to investigate the *wavelength dependence* of the visibility, differential phase, and closure phase of η Car. If we fit Hillier et al. (2001) model visibilities (Hillier et al., 2001, ApJ, 553, 837) to the observed AMBER visibilities, we obtain 50% encircled-energy diameters of 4.3, 6.5, and 9.6 mas in the $2.17\,\mu$m continuum, the He I, and the Brγ emission lines, respectively. We find good agreement between the measured visibilities and the predictions of the radiative transfer model of Hillier et al. (2001). Our observations support theoretical models of anisotropic winds from fast-rotating, luminous hot stars with enhanced high-velocity mass loss near the polar regions.

Key words: Infrared interferometry, Eta Carinae, mass loss, stellar wind

[*] Based on observations made with ESO telescopes at Paranal Observatory under programme ID 074.A-9025(A).

1   Introduction

η Car is one of the most luminous ($L \sim 4 \times 10^6 \, L_\odot$) and most massive ($M \sim 100 \, M_\odot$) unstable Luminous Blue Variables, suffering from an extremely high mass loss at a rate of $\sim 10^{-3} \, M_\odot \mathrm{yr}^{-1}$ (Davidson & Humphreys, 1997). It is surrounded by the expanding bipolar Homunculus nebula ejected during the Great Eruption in 1843. Spectroscopic studies of the Homunculus nebula showed that η Car's wind is latitude-dependent (Smith et al., 2003). van Boekel et al. (2003) resolved the aspherical wind region with NIR interferometry using the VLTI/VINCI instrument. They measured a size of approximately $5 \, \mathrm{mas}$ (50% encircled energy diameter), an axis ratio of 1.25, and a position angle of the major axis of 134°. η Car's aspherical wind can be explained by models for line-driven winds from luminous hot stars rotating near their critical speed (Owocki et al., 1996, 1998). These models predict a higher wind speed and density along the polar axis than in the equatorial plane. Hillier et al. (2001, 2006) developed a detailed spectroscopic radiative transfer model of η Car's wind which is able to explain HST/STIS spectra and can predict the wavelength dependence of the wind zone. A variety of observations suggest that the central source of η Car is a close binary (Damineli, 1996).

2   AMBER observations and data processing

AMBER is the near-infrared (J, H, K band) beam-combiner instrument of ESO's *Very Large Telescope Interferometer* (Petrov et al., 2003, 2006a,b). AMBER allows the measurement of visibilities and closure phases (Petrov et al., 2003; Millour et al., 2006). Besides the calibrated visibility and the closure phase, the spectral dispersion of AMBER also allows us to compute differential observables; namely the differential visibility and the differential phase. These quantities are particularly valuable, as they provide a measure of the spatial extent and spatial offset of the line-emitting region with respect to the continuum emission. Our AMBER η Car observations were carried out on 2004 December 26 (spectroscopic phase $\phi = 0.268$), 2005 February 25, and 2005 February 26 ($\phi = 0.299$) with the three $8.2\,\mathrm{m}$ Unit Telescopes UT2, UT3, and UT4 (Weigelt et al., 2006). Figure 1 shows two AMBER raw interferograms taken in the wavelength range around the Brγ line in HR (left) and MR mode (right). In the MR data sets, the Doppler-broadened Brγ line covers ~ 8 spectral channels, whereas in HR mode, the line is resolved by ~ 50 spectral channels. With projected baseline lengths up to $89\,\mathrm{m}$ (the exact baseline lengths are described in Figs. 2 and 3), an angular resolution of $\sim 5\,\mathrm{mas}$ was achieved in the K band. The observations were performed in the wavelength range around both the He I $2.059\,\mu\mathrm{m}$ and the Brγ $2.166\,\mu\mathrm{m}$ emission lines. For the reduction of the data, we used version 2.4 of the *amdlib* software package
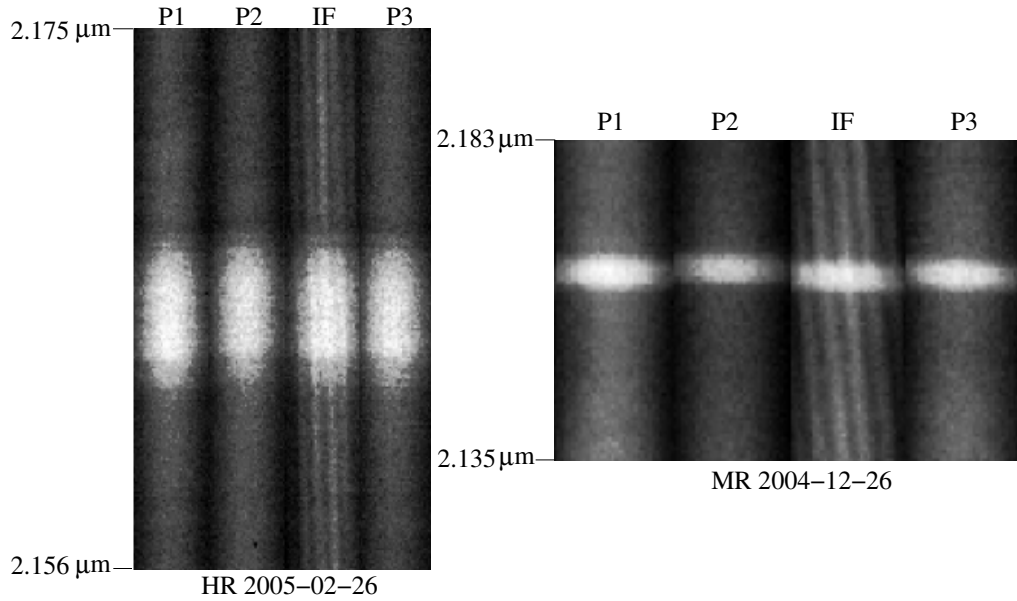
Fig. 1. Spectrally dispersed VLTI/AMBER Michelson interferograms of η Car. The two panels show the spectrally dispersed fringes (IF) as well as the photometric calibration signals from the three telescopes (P1-P3) in high (HR mode; $\lambda/\Delta\lambda = 12\,000$; left panel) and medium spectral resolution (MR mode, $\lambda/\Delta\lambda = 1\,500$; right panel). In both panels, the bright regions correspond to the Doppler-broadened Brγ line.

(this software is available from `http://amber.obs.ujf-grenoble.fr`). This software uses the P2VM (*pixel-to-visibilities matrix*) algorithm (Tatulli et al., 2006) in order to extract complex visibilities for each baseline and each spectral channel of an AMBER interferogram. From these three complex visibilities, the amplitude and the closure phase are derived.

3 Results

3.1 Wavelength dependence of the observed visibilities, differential phases, and closure phases

Figures 2 and 3 present the spectra, visibilities, differential phases, and closure phases which were derived from the interferograms. From the analysis of these measurements, we obtained the results discussed in the following sections (see Weigelt et al., 2006 for more details).
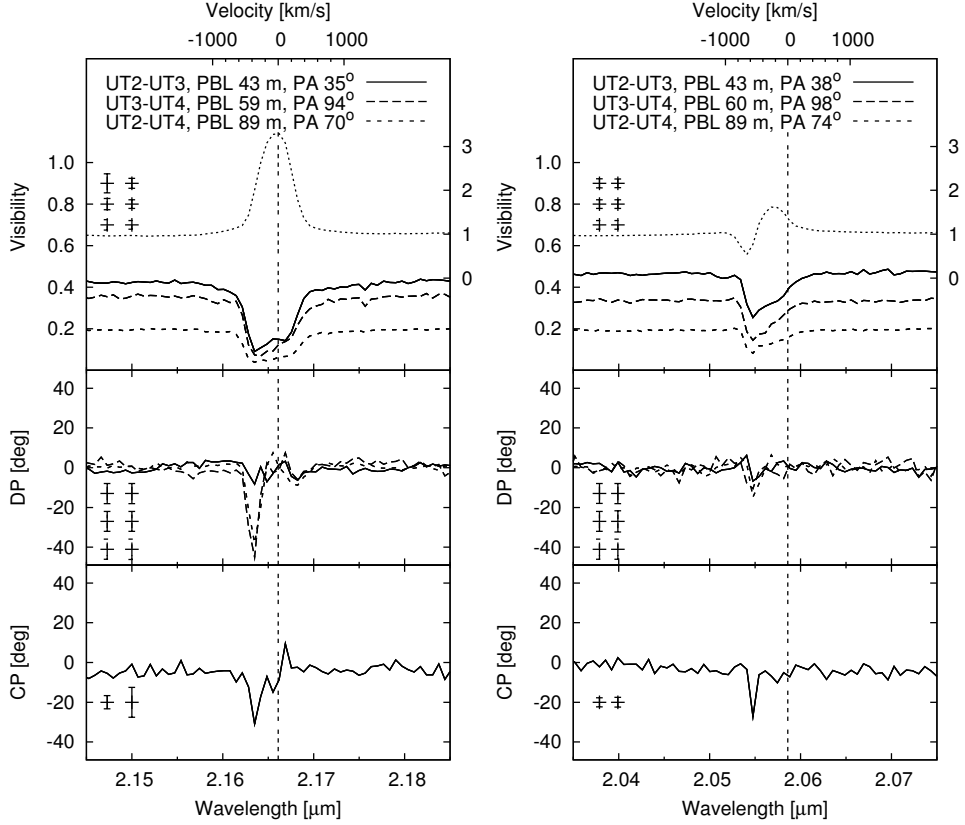
Fig. 2. AMBER observables derived from the medium resolution η Car data around the Brγ and He I lines (spectral resolution $\lambda/\Delta\lambda = 1\,500$). The curves at the top show the spectra, followed by the derived calibrated visibilities corresponding to the three baselines shown in the figures. In the second and third row, the differential phase (DP) and the closure phase (CP) are presented. The vertical line marks the rest-wavelength of Brγ ($\lambda_{\rm vac} = 2.1661\,\mu$m) and He I ($\lambda_{\rm vac} = 2.0586\,\mu$m). The small visibilities within the lines directly show that the object is more extended at wavelengths within the lines than in the continuum region. The differential phases allow the measurement of spatial offsets of the line-emitting region with respect to the continuum emission. Closure phases are a measure of asymmetry.

3.2   Comparison of the wavelength dependence of the AMBER visibilities with the model predictions by Hillier et al. (2001)

The comparison of the AMBER visibilities with the model predictions (Hillier et al., 2001) is visualized in Fig. 4. The first row displays AMBER and model spectra, while all other panels show AMBER and model visibilities for the different projected baseline lengths. As the figure reveals, the NLTE model of Hillier et al. (2001) can approximately reproduce the AMBER continuum observations. Moreover, the wavelength dependence of the model visibilities inside the Brγ line is also similar to the AMBER data. On the other hand, there is an obvious difference in the wavelength dependence of the visibility
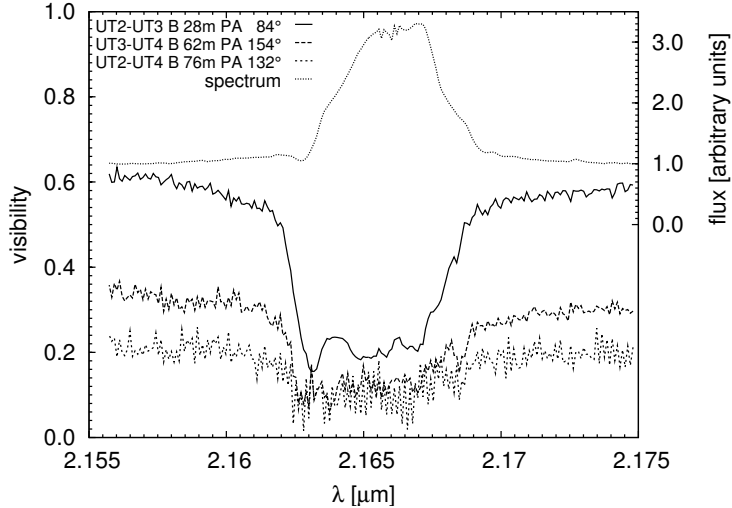
Fig. 3. Spectrum (top) and three η Car visibilities derived from our AMBER data taken with high spectral resolution of 12 000 within the Brγ line (the corresponding differential and closure phases are presented in Weigelt et al., 2006). The visibilities of the longest baseline are very noisy since lower visibilities lead to more noise.

across the He I line between the observations and the model predictions (see discussion in the caption of Fig. 4). This difference indicates that the primary wind model does not completely describe the physical origin and, hence, the spatial scale of the He I line-forming region. This discrepancy is possibly caused by He I emission from the wind-wind interaction zone between the binary components (Pittard & Corcoran, 2002; Nielsen et al., 2006).

3.3 Dependence of the visibilities on spatial frequency: AMBER observation and comparison with the Hillier et al. model predictions

Figure 5 shows the AMBER visibilities and Hillier et al. (2001) model visibilities as a function of spatial frequency (instead of visibility versus wavelength as discussed in Fig. 4) for three selected wavelengths: one continuum wavelength and the center of both the Brγ and the He I emission. The corresponding model center-to-limb intensity variations (CLVs) are also shown for illustration. As Fig. 5 reveals, we find good agreement between the visibilities (as a function of spatial frequency) measured with AMBER and the visibilities predicted by the Hillier et al. (2001) model.
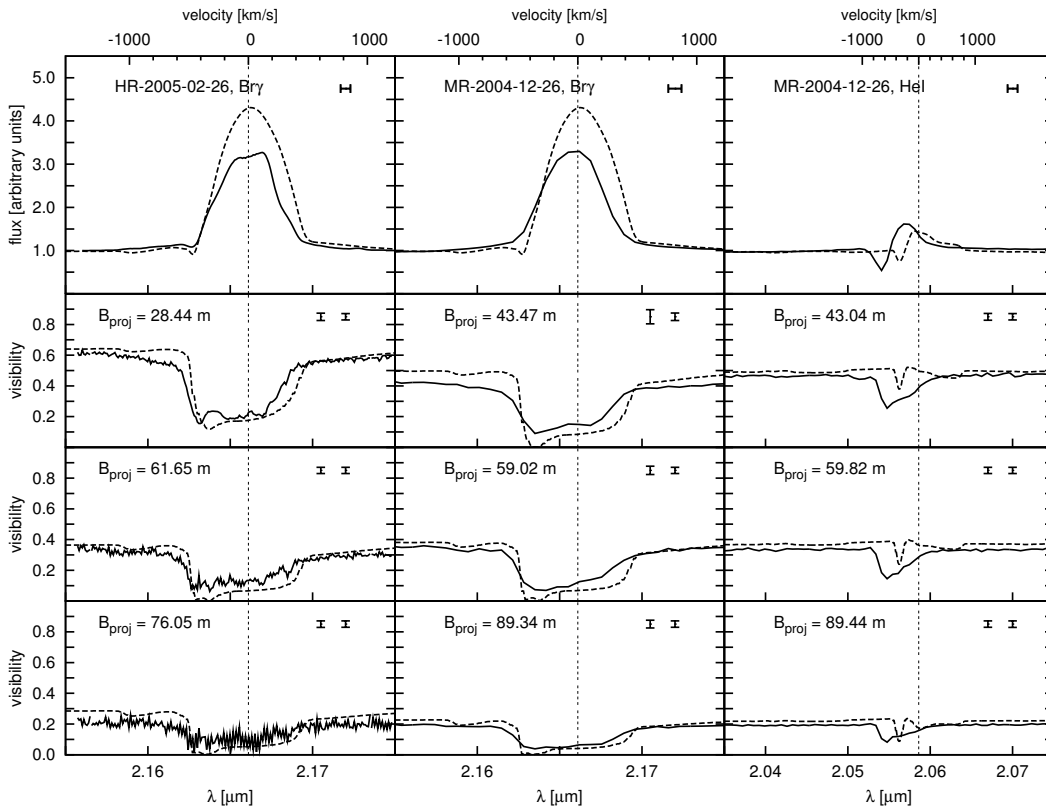
Fig. 4. Comparison of the AMBER spectra and visibilities with the model predictions of Hillier et al. (2001). The figure displays the spectra (upper row) and visibilities (lower three rows) of the AMBER measurements (solid lines) as a function of wavelength and the corresponding Hillier et al. models (dashed lines). In the case of the He I line, the differences are larger, indicating a different physical process involved in the line formation. HST/STIS observations show that the He I lines are strongly variable and blue-shifted throughout most of the 5.54-year variability period. These observations cannot be explained in the context of a spherical wind model. It now appears likely that a large fraction of the He I line emission originates in the bow shock and an ionization zone, associated with the wind-wind interaction zone in a binary system (e.g., Nielsen et al. 2006, Hillier et al. 2006).

3.4 Wavelength dependence of the diameter of η Car's optically thick wind region in the continuum, He I, and Brγ emission lines

From the wavelength dependence of the visibility, we can derive the diameter of η Car's optically thick wind region at many different wavelengths in the continuum and within the Doppler-broadened emission lines. From a Gaussian fit of the K-band continuum visibilities in the projected baseline range of 28–89 m, we obtained a FWHM diameter of 4.0 ± 0.2 mas. In the last section, we saw that there is a good agreement between the Hillier et al. model and the observations. The best fit was obtained with a slightly re-scaled version of the
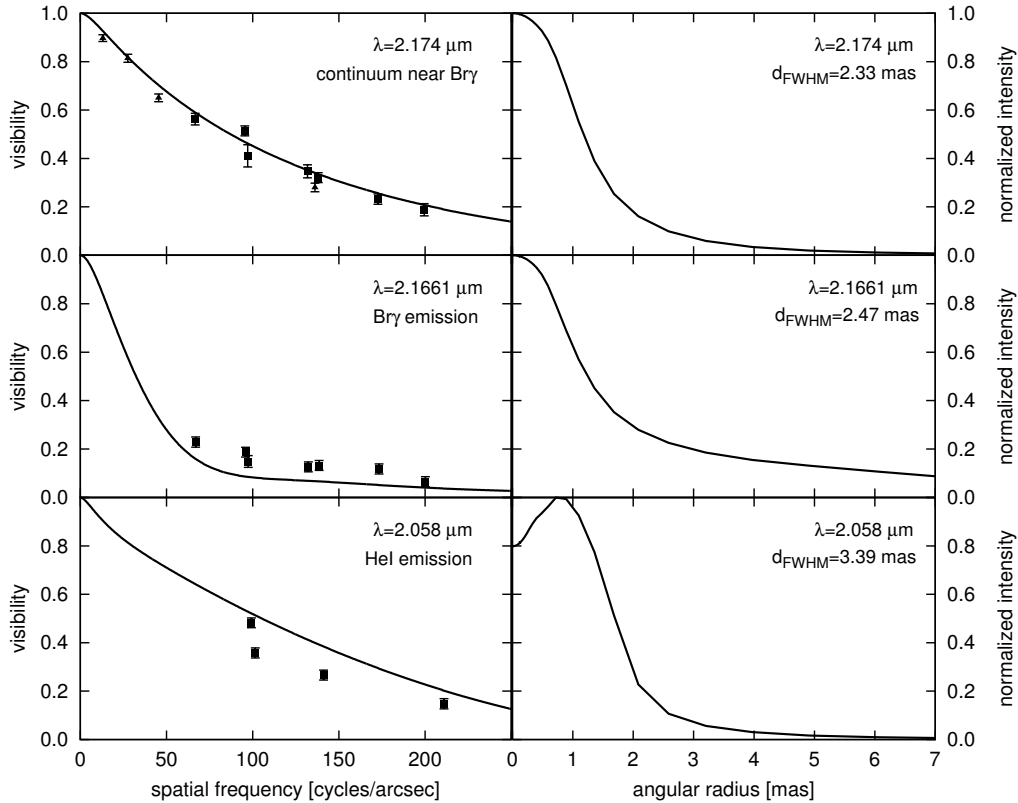
Fig. 5. Left: Comparison of η Car's AMBER visibilities (squares; baseline range 28-89 m) as a function of spatial frequency with the model predictions of Hillier et al. (2001) (lines) for three selected wavelengths: continuum (upper panel) as well as the central wavelength of the Brγ (middle), and He I emission lines (bottom). The He I visibility measurement consists of only four points since no He I observations were carried out in the high spectral resolution mode. The triangles (top, left) are the VINCI K-band measurements from van Boekel et al. (2003). Right: Center-to-limb variation of the Hillier et al. (2001) models for the wavelengths indicated by the labels. The VINCI measurements (triangles) were carried out using the 35 cm VLTI test siderostats. VINCI is a single-mode fiber instrument. Therefore, its field-of-view (FOV) is approximately equal to the Airy disk of the telescope aperture, which is ~ 1.4 arcsec in the case of the 35 cm siderostats. To account for the background contamination of the VINCI data caused by nebulosity within VINCI's large 1.4 arcsec FOV, van Boekel et al. introduced a background component (derived from NACO data) providing 55% of the total flux. Since our AMBER observations were carried out with the 8.2 m Unit Telescopes of the VLTI, the AMBER FOV was only ~ 60 mas. Thus, the background contamination of the AMBER data can be expected to be much weaker compared to the VINCI measurements. Therefore, when we finally compared the AMBER observations with the model from Hillier et al., we did not introduce a background component. In the above figure (top, left), we plot both the AMBER visibilities (squares; no background correction required) and the background-corrected VINCI data (55% background contribution; triangles). As can be seen from the figure, both the VINCI and the AMBER visibilities are in good agreement with the Hillier et al. model.

7

original Hillier et al. model. This corresponds to an observed FWHM diameter of 2.4 mas and a 50% encircled-energy diameter of 4.3 mas at $\lambda = 2.17\,\mu$m (see Weigelt et al., 2006, section 3.1 for more details of the data analysis). In the continuum around the Brγ line, we found an elongation towards position angle $120 \pm 15°$ with a projected axis ratio of 1.18 ± 0.1. This result confirms the earlier finding of van Boekel et al. (2003) using VLTI/VINCI and supports theoretical studies which predict an enhanced mass loss in polar direction for massive stars rotating close to their critical rotation rate (Owocki et al., 1996, 1998).

If we fit Hillier et al. (2001) model visibilities to the observed AMBER emission line visibilities, we obtain much larger 50% encircled-energy diameters of 6.5 and 9.6 mas in He I and the Brγ emission lines, respectively.

3.5 Differential and closure phase

For both the Brγ and the He I emission lines, we measured non-zero differential phases (DPs) and non-zero closure phases (CPs) within the emission lines (see Fig. 2), indicating a complex, asymmetric object structure. We developed a physically motivated model, which shows that the asymmetries (CPs) measured within the wings of the Brγ line are consistent with the geometry expected for an aspherical, latitude-dependent stellar wind (see Weigelt et al., 2006 for more details). Additional VLTI/AMBER measurements and radiative transfer modeling will be necessary to determine the precise parameters of the inclined aspherical wind zone.

4 Conclusion

We presented near-infrared spectro-interferometry of the enigmatic Luminous Blue Variable η Car obtained with VLTI/AMBER. Measurements with spectral resolutions of 1 500 and 12 000 were carried out in Dec. 2004 (spectroscopic phase $\phi = 0.268$) and Feb. 2005 ($\phi = 0.299$). From the measurements, we obtained spectra, visibilities, differential phases, and closure phases. From the analysis of the data, we derived the following conclusions:

- In the K-band continuum, we resolved η Car's optically thick wind. From a Gaussian fit of the K-band continuum visibilities in the projected baseline range from 28–89 m, we obtained a FWHM diameter of 4.0 ± 0.2 mas.
- When comparing the AMBER visibilities with the NLTE radiative transfer model from Hillier et al. (2001), we find good agreement between the model and observations. If we fit Hillier et al. (2001) model visibilities to the ob-

served AMBER visibilities, we obtain, for example, 50% encircled-energy diameters of 4.2, 6.5, and 9.6 mas in the $2.17\,\mu$m continuum, the He I, and the Brγ emission lines, respectively.

- In the continuum around the Brγ line, we found an asymmetry towards position angle PA $= 120 \pm 15°$ with a projected axis ratio of 1.18 ± 0.10. This result confirms the earlier finding of van Boekel et al. (2003) using VLTI/VINCI and supports theoretical studies which predict an enhanced mass loss in polar direction for massive stars rotating close to their critical rotation rate (e.g., Owocki et al., 1996, 1998).
- For both the Brγ and the He I emission lines, we measured non-zero differential phases and closure phases within the emission lines, indicating a complex, asymmetric object structure.
- We presented a physically motivated model which shows that the asymmetries (CPs) measured within the Brγ line are consistent with the geometry expected for an aspherical, latitude-dependent stellar wind.
- Using a simple binary model (not shown in this paper), we also looked for a possible binary signature in the AMBER closures phases. For separations in the range from 4 to 14 mas and arbitrary PAs, our simple model reveals a minimum K-band flux ratio of ~ 50 with a 90% likelihood (see Weigelt et al., 2006 for more details).

Repeated observations will allow us to trace changes in the observed morphology of η Car's wind zone over the spectroscopic 5.5 yr period, possibly revealing the motion of the wind-wind collision zone, as predicted by η Car's binary model. Furthermore, future AMBER observations might be sensitive enough to directly detect the hypothetical hot companion.

5   Acknowledgements

References

Damineli, A., The 5.52 Year Cycle of Eta Carinae, 1996, ApJ 460, L49

Davidson, K., & Humphreys, R.M., Eta Carinae and Its Environment, 1997, ARA&A 35, 1

Hillier, D.J., Davidson, K., Ishibashi, K., & Gull, T., On the Nature of the Central Source in η Carinae, 2001, ApJ 553, 837

Hillier, D.J., Gull, T., Nielsen, K., Sonneborn, G., Iping, R., Smith, Nathan, Corcoran, M., Damineli, A., Hamann, F.W., Martin, J.C., & Weis, K., The UV Scattering Halo of the Central Source Associated with η Carinae, 2006, ApJ 642, 1098

Millour, F., Vannier, M., Petrov, R.G., Chesneau, O., Dessart, L., Stee, P., 2006, in EAS Publications Series, in press

Nielsen, K.E., Corcoran, M.F., Gull, T.R., Hillier, D.J., Hamaguchi, K., Ivarsson, S., Lindler, D.J.,2006, ApJ in press

Owocki, S.P., Cranmer, S.R., & Gayley, K.G., Inhibition of Wind Compressed Disk Formation by Nonradial Line-Forces in Rotating Hot-Star Winds, 1996, ApJ 472, L115

Owocki, S.P., Cranmer, S.R., & Gayley, K.G., Mass Loss from Rotating Hotstars: Inhibition of Wind Compressed Disks by Nonradial Line-forces, 1998, Ap&SS 260, 149

Petrov, R.G., Malbet, F., Weigelt, G., Lisi, F., Puget, P., Antonelli, P., Beckmann, U., Lagarde, S., Lecoarer, E., Robbe-Dubois, S., Duvert, G., Gennari, S., Chelli, A., Dugue, M., Rousselet-Perraut, K., Vannier, M., & Mourard, D., Using the near infrared VLTI instrument AMBER, 2003, SPIE 4838, 924

Petrov, R. et al., 2006a, in The power of optical/IR interferometry recent scientific rsults and 2nd generation VLTI instruments (ESO, Garching, 2006) in press

Petrov, R. et al., 2006b, astro-ph 2006

Pittard, J.M., & Corcoran, M.F., In hot pursuit of the hidden companion of eta Carinae: An X-ray determination of the wind parameters, 2002, A&A 383, 636

Smith, N., Davidson, K., Gull, T.R., Ishibashi, K., & Hillier, D.J., Latitudedependent Effects in the Stellar Wind of Carinae, 2003, ApJ 586, 432

Tatulli, E. et al., 2006, astro-ph/0603046 and A&A 2007 in press

van Boekel, R., Kervella, P., Schöller, M., Herbst, T., Brandner, W., de Koter, A., Waters, L.B.F.M., Hillier, D.J., Paresce, F., Lenzen, R., & Lagrange, A.-M., Direct measurement of the size and shape of the present-day stellar wind of eta Carinae, 2003, A&A 410, L37

Weigelt, G. et al., 2006, astro-ph/0609715 and A&A 2007 in press